



Article

Altitude Control of Powered Parafoil Using Fractional Sliding-Mode Backstepping Control Combined with Extended State Observer

ErLin Zhu ¹ , Youwu Du ^{1,*}, Wei Song ¹ and Haitao Gao ² ¹ School of Electrical & Information Engineering, Jiangsu University of Technology, Changzhou 213001, China² College of Electrical and Electronic Engineering, Anhui Science and Technology University, Bengbu 233030, China

* Correspondence: duyowu@jsut.edu.cn

Abstract: This paper presents a method of altitude control of the powered parafoil with uncertainties and disturbances based on sliding-mode backstepping control combined with a linear extended state observer (LESO). First, the dynamics of a powered parafoil is derived in the longitudinal plane using its inclination angle. The problem of altitude control is converted to the issue of angle control. Next, uncertainties and disturbances are considered as a total disturbance. An LESO is used to estimate the total disturbance and form an inner-loop compensation. Backstepping control is employed to regulate the inclination angle to follow the desired value. A fractional sliding surface is introduced to the backstepping control. This ensures the transient performance of altitude control of the powered parafoil. Then, stability analysis shows that the observation errors of the LESO are bounded and the control system is uniformly ultimately bounded. Simulation results of an 8 degree-of-freedom powered parafoil illustrate that the LESO can effectively estimate the states of the system and demonstrate the validity and the superiority of the presented method.

Keywords: powered parafoil; altitude control; sliding mode backstepping; fractional calculus; LESO



Citation: Zhu, E.; Du, Y.; Song, W.; Gao, H. Altitude Control of Powered Parafoil Using Fractional Sliding-Mode Backstepping Control Combined with Extended State Observer. *Appl. Sci.* **2022**, *12*, 12069. <https://doi.org/10.3390/app122312069>

Academic Editors: Sheng Du, Xiongbo Wan, Wei Wang and Hao Fu

Received: 10 November 2022

Accepted: 23 November 2022

Published: 25 November 2022

Publisher's Note: MDPI stays neutral with regard to jurisdictional claims in published maps and institutional affiliations.



Copyright: © 2022 by the authors. Licensee MDPI, Basel, Switzerland. This article is an open access article distributed under the terms and conditions of the Creative Commons Attribution (CC BY) license (<https://creativecommons.org/licenses/by/4.0/>).

1. Introduction

The powered parafoil is a prevalent new type of air vehicle with a flex wing [1,2]. Because the engine is equipped with the payload, compared with traditional parafoils, the powered parafoil not only can glide but also cruise and climb, which traditional parafoils cannot perform [3–5]. The powered parafoil has been applied to paragliding sports, supply airdropping, pesticide spraying, and airport demisting, to name but a few, due to its excellent maneuverability [6]. In recent years, the control of powered parafoils has become a research hotspot. Compared with the horizontal control of traditional parafoils, the altitude control of powered parafoils has received extensive attention and has been a challenge because of its complex aerodynamics characteristics.

Many strategies have been proposed to control the altitude of powered parafoils. Yang et al. analyzed the flight performance of altitude control and derived the longitudinal model of a powered parafoil [7]. Aoustin and Martinenko designed a nonlinear control law for a powered parafoil based on partial feedback linearization to track a desired trajectory in the longitudinal plane [8]. Chen et al. presented a precise-gain method to handle the problem of longitudinal motion control of a powered parafoil [9]. The backstepping control was first employed to control the altitude of a powered parafoil using its lateral model [10]. Then, a fuzzy backstepping control was extended to improve the control performance of the altitude control based on a variable-gain scheme [11]. Tan et al. proposed an altitude-tracking control method for a powered parafoil using the coefficient adaptive control and the characteristic model of the parafoil [12]; however, the specification of the guidance was not provided. Zhu

et al. presented a spatial path-tracking control of a powered parafoil using the guidance theory combined with the linear active disturbance control (LADRC) [13].

The above-mentioned methods mainly used a simplified model of powered parafoils to design a controller. However, this may impose limitations on control performance as there exist strong nonlinearities and complex model couplings in powered-parafoil systems. Although Tan and Zhu employed methods of the characteristic model and LADRC that do not rely on the precise model of a powered parafoil to remove the limitations, it increases the complexity of the system design and brings difficulty in analyzing the stability of control systems. The sliding mode control (SMC) is a commonly used method for the aircraft [14,15]; however, the control is susceptible to system uncertainties and disturbances. How to effectively suppress disturbances and improve the robustness of a control system is one of the key points in system design [16,17]. On the other hand, the fractional-order theory [18,19] is widely used in industrial control systems. A fractional calculus operator shows good robustness for systems with uncertainties and external disturbances due to its hereditary and memorability.

This paper presents an alternative way to address the problem of the altitude control of a powered parafoil using the fractional sliding-mode backstepping control combined with a linear extended state observer (LESO). First, the inclination angle model of a powered parafoil is derived according to the guidance law. The altitude control of the powered parafoil is converted into the issue of the inclination angle control. Then, an LESO is used to estimate system uncertainties and exogenous disturbances. A fractional dynamic sliding-mode surface is introduced into the backstepping control to improve the transient performance of the altitude tracking. A stability criterion is derived to guarantee that virtual control variables and the error of system states are bounded. Finally, the validity of the presented method is demonstrated by simulation results of an 8-degree-of-freedom powered parafoil.

The rest of the paper is organized as follows. Section 2 derives the inclination angle model of the powered parafoil according to the guidance law. Section 3 explains the design algorithm of the control system based on the fractional sliding-mode backstepping control (FSMBC) combined with an LESO. Section 4 analyzes the stability of the control system. Section 5 shows the validity of the method through simulation results. Section 6 gives some concluding remarks and points out future work.

2. Dynamics of Powered Parafoil and Problem Formulation

Figure 1 shows the structure of a powered parafoil and its three coordinate frames, that is, $O_d X_d Y_d Z_d$ represents the earth reference frame, $O_s X_s Y_s Z_s$ represents the parafoil reference frame, and $O_w X_w Y_w Z_w$ represents the payload reference frame. The transformation between the earth reference frame and the parafoil reference frame is achieved through three Euler angles $[\psi \ \theta \ \phi]^T$; that is, ψ denotes the yaw angle, θ denotes the pitch angle, and ϕ denotes the roll angle.

The study in this paper focuses on the altitude control of a powered parafoil that involves the relative motion between a parafoil and a payload. The dynamics model is established according to the Kirchhoff motion equation. The specific modeling process and model parameters can be found in [20].

The inclination angle σ of the powered parafoil is defined as the angle between the velocity and the horizontal plane, shown as

$$\sigma = \arctan\left(\frac{-\dot{z}}{\sqrt{\dot{x}^2 + \dot{y}^2}}\right), \quad (1)$$

where $[x \ y \ z]^T$ is the position vector in the earth reference frame.

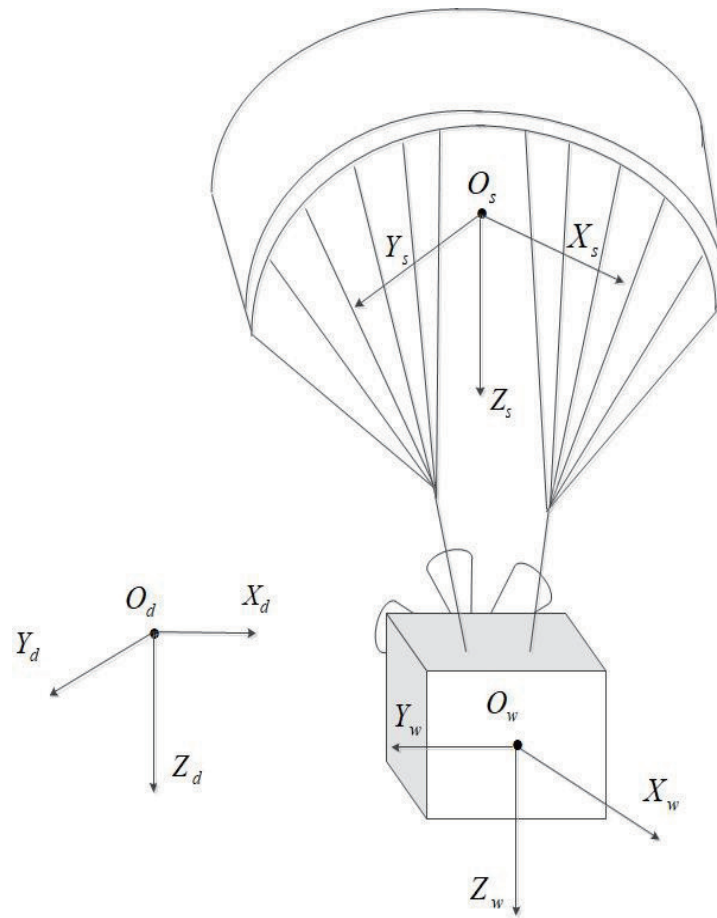


Figure 1. The structure of the powered parafoil and coordinate frames.

Lemma 1 ([13]). *The vertical error e_h between the powered parafoil and the desired point p_p is global uniformly asymptotically stable and local exponential stable, if the inclination angle of the powered parafoil changes with the following guidance law*

$$\sigma_d = \arctan\left(\frac{e_h}{k_h}\right), \tag{2}$$

where $e_h = H_d - H$ and k_h is an adjustable parameter. H_d and H are the desired altitude and actual altitude of the powered parafoil, respectively.

According to Lemma 1, the altitude control of the powered parafoil can be converted to the control of the inclination angle.

The velocity transformation from the parafoil frame to the earth frame can be described as

$$\begin{bmatrix} \dot{x} \\ \dot{y} \\ \dot{z} \end{bmatrix} = \mathbf{R}_{p-e} \begin{bmatrix} u_s \\ v_s \\ w_s \end{bmatrix}, \tag{3}$$

where $[u_s \ v_s \ w_s]^T$ is the velocity vector in the parafoil frame and the transformation matrix

$$\mathbf{R}_{p-e} = \begin{bmatrix} \cos \theta \cos \psi & \sin \phi \sin \theta \cos \psi - \cos \phi \sin \psi & \cos \phi \sin \theta \cos \psi + \sin \phi \sin \psi \\ \cos \theta \sin \psi & \sin \phi \sin \theta \sin \psi + \cos \phi \cos \psi & \cos \phi \sin \theta \sin \psi - \sin \phi \cos \psi \\ -\sin \theta & \sin \phi \cos \theta & \cos \phi \cos \theta \end{bmatrix}. \tag{4}$$

If the motion of the longitudinal plane is considered, then it is easy to obtain

$$v_s = 0, \dot{y} = 0, \psi = 0, \phi = 0. \tag{5}$$

Substituting (4) and (5) into (3) yields

$$\dot{x} = u_s \cos \theta + w_s \sin \theta, \tag{6}$$

$$\dot{z} = -u_s \sin \theta + w_s \cos \theta. \tag{7}$$

Choose the inclination angle σ of the powered parafoil as the state variable of the system. According to (1), (6), and (7), the first derivative of σ is

$$\dot{\sigma} = \dot{\theta} + \frac{\dot{u}_s w_s - u_s \dot{w}_s}{u_s^2 + w_s^2}. \tag{8}$$

Let f_s be the derivative of $\frac{\dot{u}_s w_s - u_s \dot{w}_s}{u_s^2 + w_s^2}$. The second derivative of σ is obtained as

$$\ddot{\sigma} = \ddot{\theta} + f_s. \tag{9}$$

For the altitude control of the powered parafoil, the only control variable that affects the flight velocity is the thrust u provided by the power propulsion. According to the nonlinear dynamics model of the powered parafoil [20], the thrust control variable is coupled in f_s , which increases the difficulty in the design of the controller. To facilitate the design of the control system, the control variable should be separated out. Rewrite (9) as

$$\begin{aligned} \ddot{\sigma} &= \ddot{\theta} + f_s - bu + bu \\ &= f + bu, \end{aligned} \tag{10}$$

where $f = \ddot{\theta} + f_s - bu$ is viewed as a total disturbance.

The state space model of the dynamics of σ is obtained as

$$\begin{aligned} \dot{x}_1 &= x_2 \\ \dot{x}_2 &= f + bu \\ x_1 &= \sigma. \end{aligned} \tag{11}$$

The main objective of this study is to minimize the error of the inclination angle despite of the influence of system uncertainties of the dynamics model and external disturbances on the system. In the next section, a new control scheme is proposed to handle this issue. The LESO is used to estimate uncertainties and disturbance. A fractional sliding-mode backstepping control law is devised to improve control performance and the stability of the system.

3. Design of Control System

In this section, a method of FSMBC with LESO is proposed for the altitude control of a powered parafoil. The configuration of the control system of the powered parafoil is shown in Figure 2, which consists of guidance-based path following, FSMBC, LESO, and the powered parafoil. The outer-loop is a guidance loop, from where the desired inclination angle (2) is obtained according to altitude signals. The inner-loop is the control loop of the inclination angle. FSMBC is adopted, and LESO is used to observe and eliminate the total disturbance.

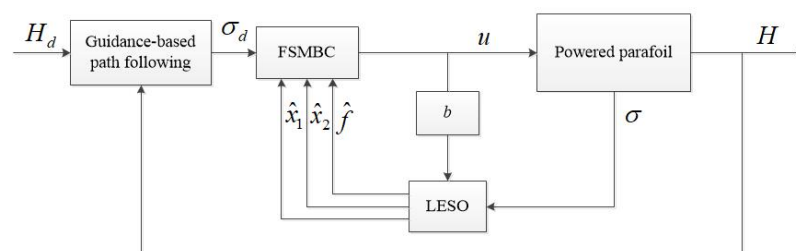


Figure 2. Configuration of the control system of the powered parafoil.

3.1. Design of LESO

Assume $\dot{f}_{total} = h$. Rewrite (11) as

$$\dot{X} = A_1 X + B_1 u + B_2 h, \tag{12}$$

where $A_1 = \begin{bmatrix} 0 & 1 & 0 \\ 0 & 0 & 1 \\ 0 & 0 & 0 \end{bmatrix}$, $B_1 = [0 \ b \ 0]^T$, $B_2 = [0 \ 0 \ 1]^T$, $X = [x_1 \ x_2 \ f]^T$. Construct an LESO as

$$\dot{\hat{X}} = A_1 \hat{X} + B_1 u + L(X - \hat{X}), \tag{13}$$

where $\hat{X} = [\hat{x}_1 \ \hat{x}_2 \ \hat{f}]^T$ is the estimated value of X and L is the gain matrix of LESO, which is given by

$$L = \begin{bmatrix} l_1 & 0 & 0 \\ l_2 & 0 & 0 \\ l_3 & 0 & 0 \end{bmatrix}. \tag{14}$$

Let \tilde{e} represent the estimated error of the LESO. We have

$$\tilde{e} = X - \hat{X}. \tag{15}$$

According to (12), (13), and (15), the following differential equation with respect to \tilde{e} can be obtained as

$$\dot{\tilde{e}} = A_2 \tilde{e} + B_2 h, \tag{16}$$

where $A_2 = A_1 - L$.

Assume that h is bounded, namely there exists a positive constant M_1 such that $|h| \leq M_1$. The estimated error of the LESO is always bounded, that is, there exists a positive constant M_2 such that $\|\tilde{e}\| \leq M_2$ holds [21].

3.2. Design of Fractional Sliding Mode Backstepping Control

The estimated states \hat{x}_1 and \hat{x}_2 of the LESO are used in the design of fractional sliding-mode backstepping control. Define the tracking error of the inclination angle as

$$e_1 = \sigma_d - \hat{x}_1. \tag{17}$$

Calculating the derivative of (17) yields

$$\begin{aligned} \dot{e}_1 &= \dot{\sigma}_d - \dot{\hat{x}}_1 \\ &= \dot{\sigma}_d - \hat{x}_2. \end{aligned} \tag{18}$$

Define an auxiliary error e_2 as

$$e_2 = x_{2d} - \hat{x}_2. \tag{19}$$

where x_{2d} is a virtual control variable. It is easy to obtain

$$\dot{e}_1 = e_2 + \dot{\sigma}_d - x_{2d}. \tag{20}$$

According to the error system, let the virtual control variable satisfy

$$x_{2d} = \dot{\sigma}_d + k_1 e_1, \tag{21}$$

where $k_1 \in R^+$ is the feedback gain.

To avoid differential explosion, the algorithm of dynamic surface control is employed. Designing a low-pass filter and passing the virtual control variable x_{2d} through it yield

$$T \dot{\hat{x}}_{2d} + \hat{x}_{2d} = x_{2d}, \hat{x}_{2d}(0) = x_{2d}(0), \tag{22}$$

where T is the time constant of the filter and \hat{x}_{2d} is the filtered virtual control variable. Define the filter error as

$$\tilde{x}_{2d} = \hat{x}_{2d} - x_{2d}. \tag{23}$$

Calculating the derivative of (23) along (22) yields

$$\begin{aligned} \dot{\tilde{x}}_{2d} &= \dot{\hat{x}}_{2d} - \dot{x}_{2d} \\ &= -\frac{1}{T}\tilde{x}_{2d} - (\ddot{\sigma}_d + k_1\dot{e}_1) \\ &= -\frac{1}{T}\tilde{x}_{2d} + B(\ddot{\sigma}_d, \dot{e}_1), \end{aligned} \tag{24}$$

where $B(\ddot{\sigma}_d, \dot{e}_1)$ is a function about $\ddot{\sigma}_d$ and \dot{e}_1 . There exists a positive constant B_M such that $|B| \leq B_M$ [22]. Substituting (21) into (20) yields

$$\dot{e}_1 = e_2 - k_1e_1. \tag{25}$$

Choose a Lyapunov candidate to be

$$V_1 = \frac{1}{2}e_1^2. \tag{26}$$

It is easy to obtain

$$\dot{V}_1 = e_1\dot{e}_1 = e_1(e_2 - k_1e_1) = e_1e_2 - k_1e_1^2. \tag{27}$$

In this study, the methodology of the sliding surface and the backstepping control is used to ensure that e_1 and e_2 converge quickly. Moreover, the fractional calculus operator is employed to improve transient performance in the design of a sliding mode surface, which is denoted by

$$s = \lambda_1e_1 + {}_aD_t^\alpha e_2. \tag{28}$$

where λ_1 is the sliding surface gain and ${}_aD_t^\alpha$ is the calculus operator

$${}_aD_t^\alpha = \begin{cases} \frac{d^\alpha}{dt^\alpha} & Re(\alpha) > 0 \\ 1 & Re(\alpha) = 0 \\ \int_a^t d(\tau)^{-\alpha} & Re(\alpha) < 0. \end{cases} \tag{29}$$

In (29), α is the order of the operator and can be used to adjust transient performance of the control system. For simplicity of implementation, we choose the Caputo fractional calculus [23–25]

$${}_aD_t^\alpha f(t) = \frac{1}{\Gamma(m - \alpha)} \int_a^t \frac{f^m(\tau)}{(t - \tau)^{1+\alpha-m}} d\tau, m - 1 < \alpha < m, \tag{30}$$

where $\Gamma(\cdot)$ is Gamma Function, $\Gamma(\eta) = \int_0^\infty e^{-t}t^{\eta-1}dt$ and m is the least integer that is not less than α . The fractional differential operation is transformed to the particular form of integral operation; therefore, the fractional calculus has the heritability and the memorability. To simplify the notation, let D^α represent ${}_0D_t^\alpha$. This should not cause confusion.

In order to make the system state converge to the sliding-mode surface and further weaken the chattering of the system, the fractional reaching law is designed as

$$D^\beta s = -\epsilon s \operatorname{sgn}(s), \tag{31}$$

where ϵ is a positive constant. According to the properties of fractional calculus, we have

$$\dot{s} = D^{1-\beta}(-\epsilon \operatorname{sgn}(s)). \tag{32}$$

Taking the derivative of the fractional sliding-mode surface yields

$$\dot{s} = \lambda_1 \dot{e}_1 + D^\alpha \dot{e}_2. \tag{33}$$

Choose a Lyapunov candidate to be

$$V_2 = V_1 + \frac{1}{2}s^2. \tag{34}$$

Calculating the derivative of V_2 gives

$$\begin{aligned} \dot{V}_2 &= \dot{V}_1 + s\dot{s} \\ &= e_1 e_2 - k_1 e_1^2 + s(\lambda_1 \dot{e}_1 + D^\alpha \dot{e}_2) \\ &= e_1 e_2 - k_1 e_1^2 + s(\lambda_1 \dot{e}_1 + D^\alpha (\dot{x}_{2d} - f - bu)). \end{aligned} \tag{35}$$

The control law is designed to be

$$u = \frac{1}{b} \left(\dot{x}_{2d} - \hat{f} + D^{-\alpha} \left(\lambda_1 \dot{e}_1 + ks + D^{1-\beta} \epsilon \operatorname{sgn}(s) \right) \right), \tag{36}$$

where k is a positive adjustable parameter.

4. Stability Analysis

Theorem 1. *The errors of the system (11) with the control law (36) are uniformly ultimately bounded, if the parameter $k < 1$ and the time constant of the filter $T < 2$.*

Proof of Theorem 1. Assume there exists a positive definite matrix \mathbf{P} such that $\mathbf{A}_2^T \mathbf{P} + \mathbf{P} \mathbf{A}_2 = -\mathbf{I}$. Construct a Lyapunov function

$$V = \frac{1}{2}e_1^2 + \frac{1}{2}s^2 + \frac{1}{2}\tilde{x}_{2d}^2 + \tilde{\mathbf{e}}^T \mathbf{P} \tilde{\mathbf{e}}. \tag{37}$$

Substituting (36) into (35) yields

$$\dot{V} = e_1 e_2 - k_1 e_1^2 + s(\hat{f} - f - ks - D^{1-\beta} \epsilon \operatorname{sgn}(s)) + \tilde{x}_{2d} \dot{\tilde{x}}_{2d} + 2\tilde{\mathbf{e}}^T \mathbf{P} \dot{\tilde{\mathbf{e}}}. \tag{38}$$

A proper selection of the gain L ensures that the error dynamics of the LESO is stable. Thus, it is reasonable to assume that $\hat{f} \approx f_{total}$. Then, rewrite (38) as

$$\begin{aligned} \dot{V} &= e_1 e_2 - k_1 e_1^2 - s(ks + D^{1-\beta} \epsilon \operatorname{sgn}(s)) + \tilde{x}_{2d} \dot{\tilde{x}}_{2d} + 2\tilde{\mathbf{e}}^T \mathbf{P} \dot{\tilde{\mathbf{e}}} \\ &= e_1 e_2 - k_1 e_1^2 - ks^2 - sD^{1-\beta} \epsilon \operatorname{sgn}(s) + \tilde{x}_{2d} \dot{\tilde{x}}_{2d} + 2\tilde{\mathbf{e}}^T \mathbf{P} \dot{\tilde{\mathbf{e}}} \\ &= e_1 e_2 - k_1 e_1^2 + (1 - k)s^2 - s^2 + s\dot{s} + \tilde{x}_{2d} \dot{\tilde{x}}_{2d} + 2\tilde{\mathbf{e}}^T \mathbf{P} \dot{\tilde{\mathbf{e}}}. \end{aligned} \tag{39}$$

Let $e_{12} = [e_1 \quad e_2 \quad D^\alpha e_2]^T$, and choose a symmetric matrix \mathbf{Q}

$$\mathbf{Q} = \begin{bmatrix} k_1 + (k - 1)\lambda_1^2 & -0.5 & (k - 1)\lambda_1 \\ -0.5 & 0 & 0 \\ (k - 1)\lambda_1 & 0 & k - 1 \end{bmatrix} \tag{40}$$

to make

$$\begin{aligned} e_{12}^T \mathbf{Q} e_{12} &= -e_1 e_2 + k_1 e_1^2 - (1 - k)(\lambda_1 e_1 + D^\alpha e_2)^2 \\ &= -e_1 e_2 + k_1 e_1^2 - (1 - k)s^2 \end{aligned} \tag{41}$$

hold. Substituting (41) into (39) yields

$$\dot{V} = -e_{12}^T Q e_{12} - s^2 + s\dot{s} + \tilde{x}_{2d}\dot{\tilde{x}}_{2d} + 2\tilde{e}^T P \dot{\tilde{e}}. \tag{42}$$

Calculating the determinant of Q gives

$$|Q| = -0.25(k - 1). \tag{43}$$

It can be seen that k should satisfy $k < 1$ to guarantee that $|Q| > 0$ holds. Thus $-e_{12}^T Q e_{12} < 0$ holds and there exists a positive constant μ such that the inequality

$$\dot{V} \leq -\mu e_1^2 - s^2 + s\dot{s} + \tilde{x}_{2d}\dot{\tilde{x}}_{2d} + 2\tilde{e}^T P \dot{\tilde{e}} \tag{44}$$

is satisfied.

Assume \dot{s} is bounded and $|\dot{s}| \leq S_M$, where S_M is a positive constant. According to Yong’s inequality, it is easy to obtain

$$\begin{aligned} \tilde{x}_{2d}\dot{\tilde{x}}_{2d} &= -\frac{1}{T}\tilde{x}_{2d}^2 + \tilde{x}_{2d}B \\ &\leq -\frac{1}{T}\tilde{x}_{2d}^2 + |\tilde{x}_{2d}B| \\ &\leq -\frac{1}{T}\tilde{x}_{2d}^2 + |\tilde{x}_{2d}|B_M \\ &\leq -\frac{1}{T}\tilde{x}_{2d}^2 + \frac{1}{2}\tilde{x}_{2d}^2 + \frac{1}{2}B_M^2 \end{aligned} \tag{45}$$

and

$$\begin{aligned} s\dot{s} &\leq \frac{1}{2}s^2 + \frac{1}{2}\dot{s}^2 \\ &\leq \frac{1}{2}s^2 + \frac{1}{2}S_M^2. \end{aligned} \tag{46}$$

According to (16), we have

$$\begin{aligned} 2\tilde{e}^T P \dot{\tilde{e}} &= 2\tilde{e}^T P(A_2\tilde{e} + B_2h) \\ &= -\tilde{e}^T \tilde{e} + 2\tilde{e}^T P B_2 h \\ &\leq -\tilde{e}^T \tilde{e} + 2M_1 M_2 \|P B_2\|. \end{aligned} \tag{47}$$

Substituting (45)–(47) into (44) yields

$$\dot{V} \leq -\mu e_1^2 - \frac{1}{2}s^2 - \left(\frac{1}{T} - \frac{1}{2}\right)\tilde{x}_{2d}^2 - \tilde{e}^T \tilde{e} + \frac{1}{2}S_M^2 + \frac{1}{2}B_M^2 + 2M_1 M_2 \|P B_2\|. \tag{48}$$

Assume $\frac{1}{T} - \frac{1}{2} > 0$. Then, let $\tau = \min\left\{2\mu, 1, \frac{2}{T} - 1, \frac{1}{\lambda_{\max}(P)}\right\}$, where $\lambda_{\max}(P)$ denotes the maximum eigenvalue of P . Rewrite (48) as

$$\dot{V} \leq -\tau V + v, \tag{49}$$

where $v = \frac{1}{2}S_M^2 + \frac{1}{2}B_M^2 + 2M_1 M_2 \|P B_2\|$.

Solving the differential inequality (49) yields

$$V \leq \frac{v}{\tau} + \left[V(0) + \frac{v}{\tau}\right]e^{-\tau t}. \tag{50}$$

This indicates that V is uniformly ultimately bounded.

It can be concluded that $|e_1| \leq \sqrt{\frac{2v}{\tau}}$, $|s| \leq \sqrt{\frac{2v}{\tau}}$, $|\tilde{x}_{2d}| \leq \sqrt{\frac{2v}{\tau}}$, $\|\tilde{e}\| \leq \sqrt{\frac{v}{\lambda_{\min}(\mathbf{P})\tau}}$, where $\lambda_{\min}(\mathbf{P})$ denotes the minimum eigenvalue of \mathbf{P} . All signals in the powered-parafoil control system are uniformly ultimately bounded. This completes the proof. \square

5. Simulation Verification

Simulation results of the altitude control of an 8-degree-of-freedom powered parafoil were used to verify the validity of the presented method. The main structure parameters of the powered parafoil are shown in Table 1. Simulation results are compared with LADRC and SMC in [13].

Table 1. Structure parameters of the powered parafoil.

Parameter	Value/Unit
Span	10.5/m
Chord	3.1/m
Aspect ratio	3
Area of canopy	33/m ²
Length of lines	6.8/m
Rigging angle	10/deg
Mass of canopy	10/kg
Mass of payload	80/kg
Characteristic area of drag of payload	0.6/m ²

The bandwidth parameterization method was used to design the gain of the LESO.

$$l_1 = 90, l_2 = 2700, l_3 = 2700.$$

The time constant of the filter was selected to be $T = 0.025$ s.

The parameters of the designed fractional sliding mode backstepping controller were designed to be

$$\lambda_1 = 0.16, k_1 = 0.02, k = 0.015, \alpha = 0.82, \beta = 0.36, \epsilon = 0.01.$$

The saturation of the control input was considered. The maximum thrust provided by the engine was limited to 400 N.

The initial altitude of the powered parafoil was set to be 2000 m and the desired altitude H_d was set to be 1970 m. A gust disturbance (2 m/s) along the negative direction of the Z axis was added to the system during 100–115 s, which is shown in Figure 3.

Figure 4 shows the observed results of the LESO. The outputs of the observer can effectively observe each state of the system. For comparison, simulations for the LADRC and the SMC in [13] were also carried out. The design of the LADRC and the SMC was the same as that in [13]. Figure 5 shows the attitude angles of the powered parafoil in the longitudinal plane for the three methods. The pitch angles remained at 9° after the powered parafoil entered the steady-state. The pitch angles oscillated violently when the parafoil suffered from the gust disturbance. It can be seen that the transient performance is better for the parafoil with FSMBC than for that with other two methods.

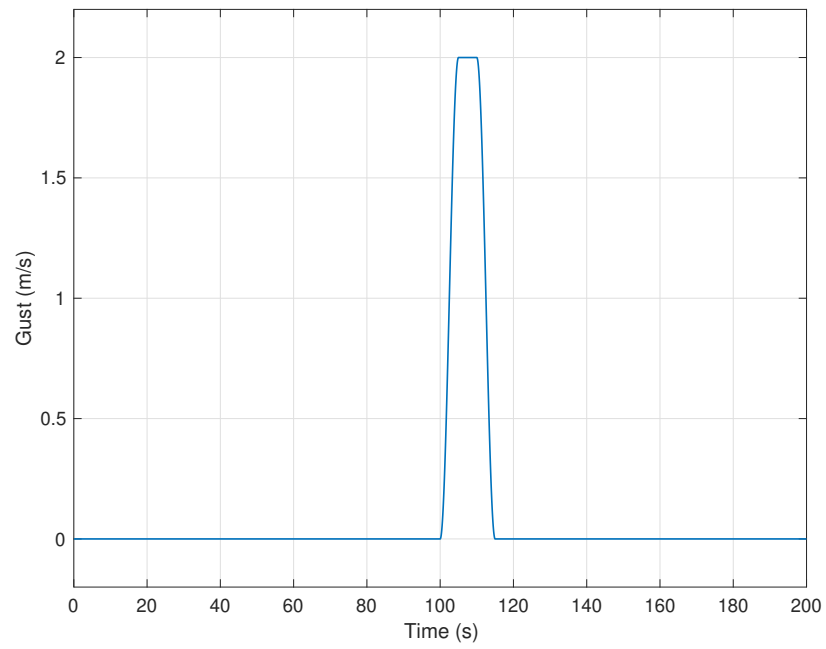


Figure 3. The gust disturbance.

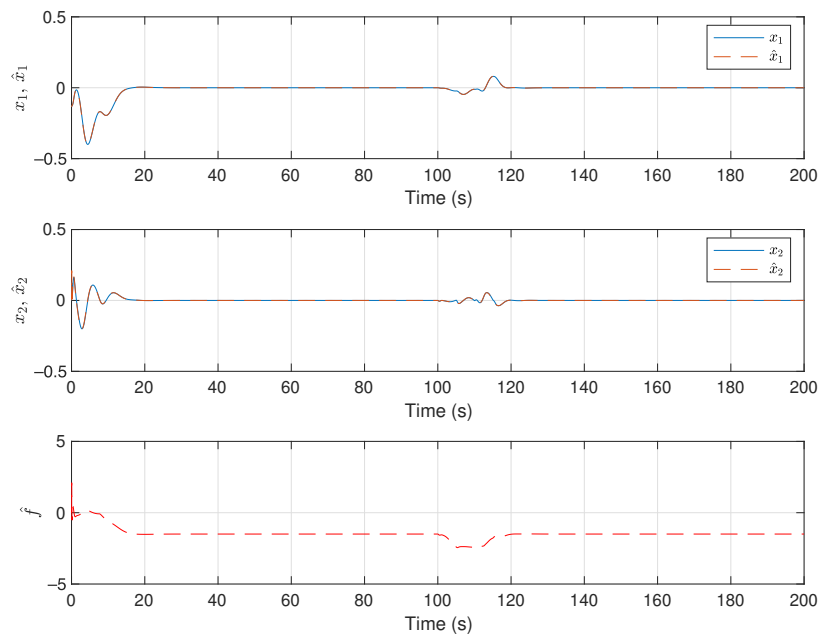


Figure 4. Observed results of LESO.

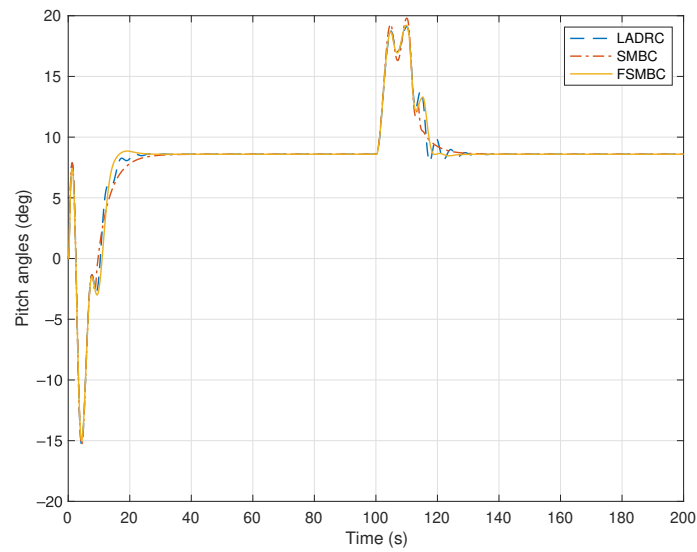


Figure 5. Simulation results of the pitch angle.

Figure 6 illustrates the simulation results of the altitude control. The altitude of the powered parafoil with the FSMBC stabilized at 1970 m after 13 s. The convergence time was less than that of the LADRC and SMC. Moreover, the recovery speed against the disturbance is faster for the FSMBC than for the LADRC and SMC. Compared with other two control methods, there exists about 1.4 m steady-state error for the SMC due to the lack of ESO. It can be seen from Figure 7 that the thrust input for the FSMBC stabilizes at 18 s, and the convergence speed is faster than that for the LADRC and SMC. It is obvious that the thrust input for the FSMBC is smoother than that for the LADRC and SMC. This is beneficial to energy saving and system stability. The SMC used a traditional integer order sliding surface, which caused the thrust input fluctuated. The specific performance indexes are shown in Table 2.

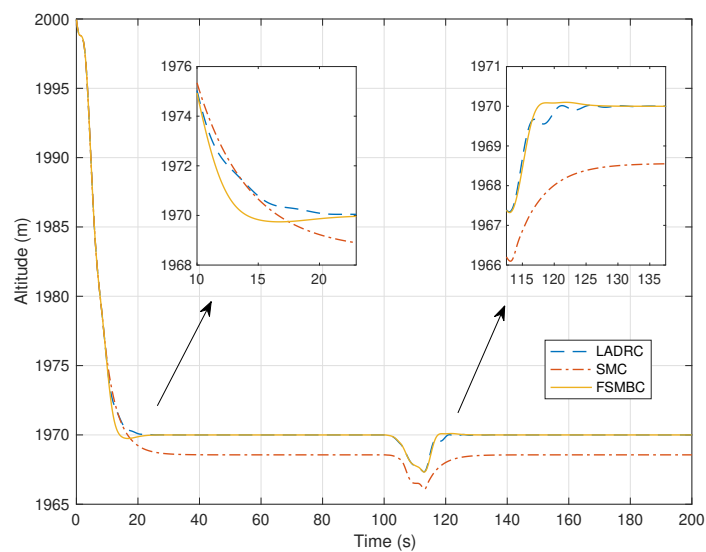


Figure 6. Simulation results of altitude control by LADRC, SMC, and FSMBC.

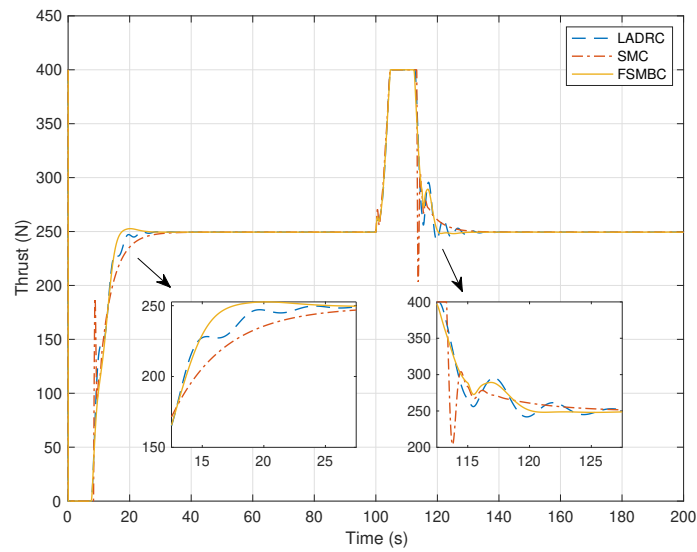


Figure 7. Thrust inputs for LADRC, SMC, and FSMBC.

Table 2. The performance indexes of the control system.

	FSMBC	LADRC	SMC
Transient time of the altitude	13 s	16 s	18 s
Steady-state error	0.00 m	0.00 m	1.44 m
Transient time of the thrust	18 s	29 s	35 s
Settling time under disturbance	16 s	20 s	28 s

The variable altitude control of the powered parafoil were also considered. The desired altitude changed from 1970 m to 1960 m at 50 s. Simulation results are shown in Figures 8–11.

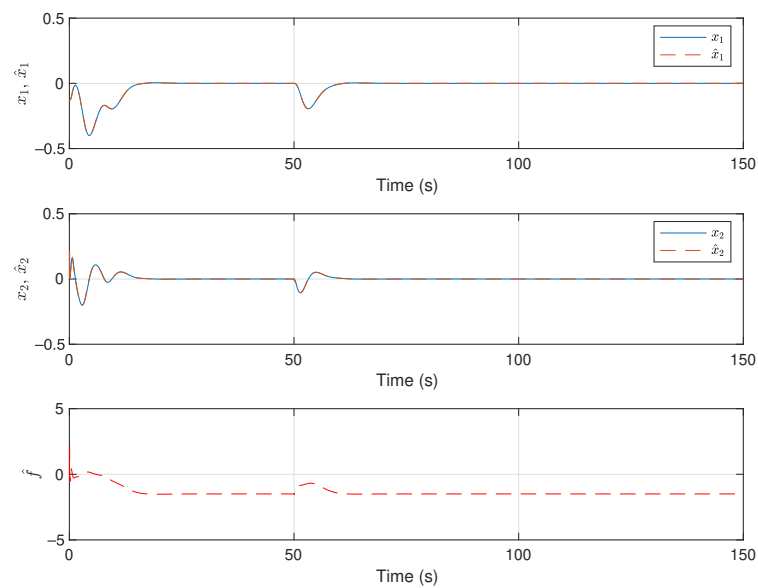


Figure 8. Observed results of LESO for variable altitude control.

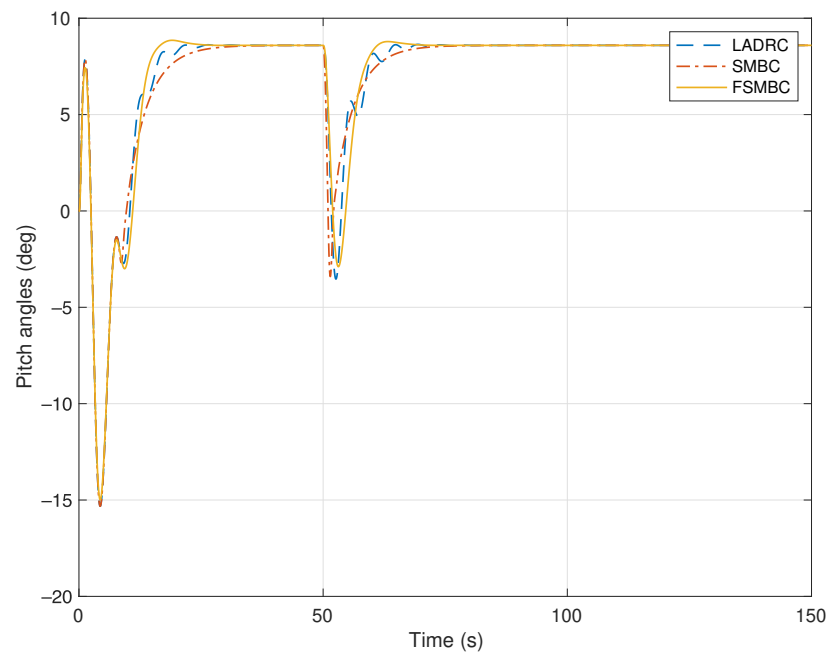


Figure 9. Simulation results of the pitch angle for variable altitude control.

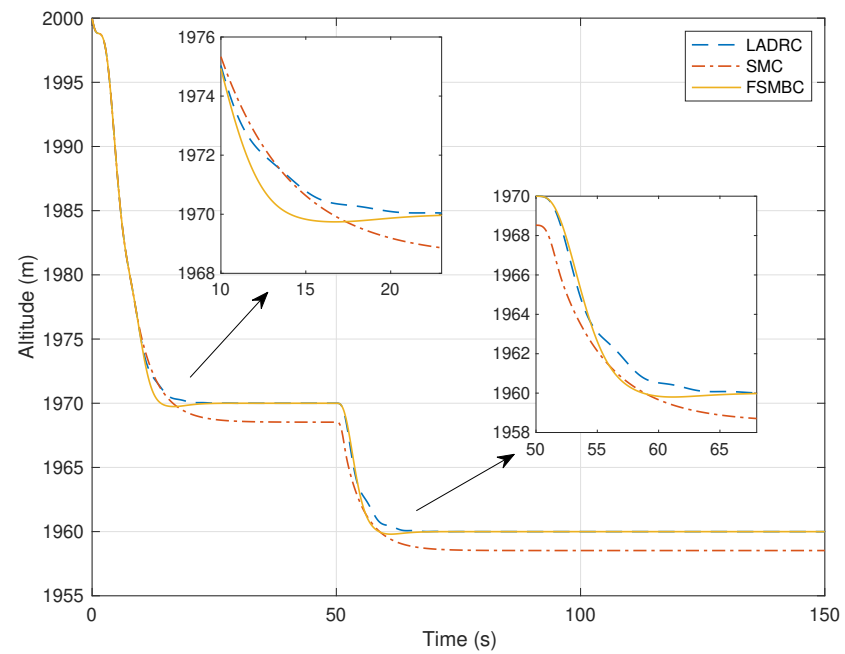


Figure 10. Simulation results of altitude control by LADRC, SMC, and FSMBC for variable altitude control.

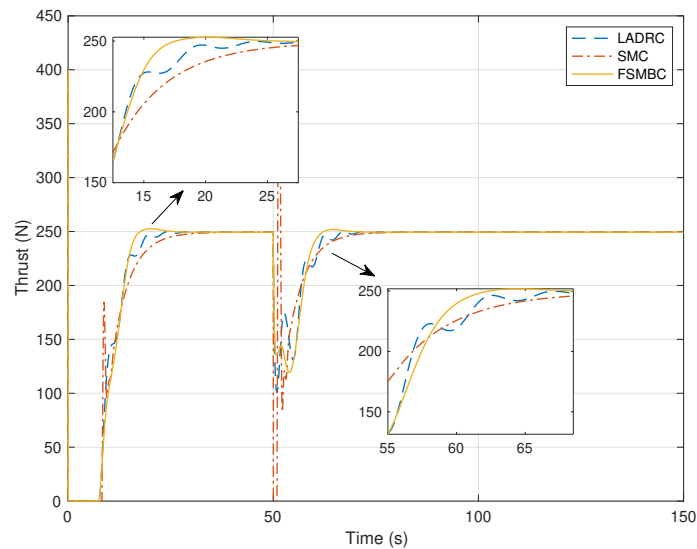


Figure 11. Thrust inputs for LADRC, SMC, and FSMBC for variable altitude control.

Figure 8 shows the observed results of the LESO for variable altitude control. The simulation results of pitch angles are shown in Figure 9. When the desired altitude changed to 1960 m, the altitude of the powered parafoil decreased accordingly and the pitch angle deviated from the steady-state value. When the altitude approached to the desired value, the pitch angle returned to the previous steady-state value. Figure 10 shows that the transient performance is better for the FSMBC than for the LADRC and SMC. The settling time is 8 s for the FSMBC and 11 s for the LADRC and SMC. Figure 11 shows that the thrust input for the SMC vibrates more violently than that of the LADRC and FSMBC during the transient response. The proposed method, that is, FSMBC, achieved good rapidity and smoothness. The performance indexes are shown in Table 3. The transient times of the altitude and the thrust are the same as in Table 2.

Table 3. The performance indexes of the control system for variable altitude control.

	FSMBC	LADRC	SMC
Steady-state error	0.00 m	0.00 m	1.47 m
Settling time of variable altitude	8 s	11 s	11 s

According to the two simulation experiments, due to the lack of ESO, SMC cannot observe and compensate the total disturbance of the system such that there exists the steady-state error. FSMBC adopts the fractional sliding-mode surface such that dynamic characteristics are better than LADRC and SMC, and the control curve is smoother due to the fractional reaching law.

6. Conclusions

This paper addressed the problem of the altitude control of the powered parafoil. The dynamic model of the powered parafoil was derived and converted into the second-order model of the inclination angle. The LESO was devised to estimate the unmodeled dynamics and the exogenous disturbance. Consequently, the estimate was used for compensation in the control law. The fractional sliding-mode surface was employed in the design of the backstepping design to improve the transient performance of the altitude control. The stability criterion of the control system was derived using the Lyapunov method. Simulation results demonstrated the validity and the superiority of the presented method. It was shown that the control performance was better for the FSMBC than for the LADRC and SMC. However, only longitudinal control problem of the powered parafoil was studied

in this paper without considering the coupling problem in the horizontal plane. Future work will be focused on the horizontal orientation control of the powered parafoil.

Author Contributions: Conceptualization, E.Z.; methodology, E.Z. and Y.D.; validation and writing—original draft preparation, E.Z.; writing—review, editing, and supervision, Y.D.; funding acquisition, Y.D., W.S., and H.G. All authors have read and agreed to the published version of the manuscript.

Funding: This research was funded by Changzhou Sci&Tech Program under Grant CJ20220068, by Natural Science Foundation of Jiangsu Province under Grant BK20221404, by the Talent Introduction Project of Jiangsu University of Technology under Grant KYY22005, by National Nature Science Foundation under Grant 61803186 and by Anhui University Top-notch Talents Academic Funding Project under Grant gxbjZD2020079.

Institutional Review Board Statement: Not applicable.

Informed Consent Statement: Not applicable.

Data Availability Statement: Not applicable.

Acknowledgments: The authors acknowledge the support from the Robotics and High-end Equipment Innovation Team of the School of Electrical & Information Engineering in Jiangsu University of Technology.

Conflicts of Interest: The authors declare no conflict of interest.

References

1. Chambers, J. Longitudinal Dynamic Modeling and Control of Powered Parachute Aircraft. Ph.D. Thesis, Rochester Institute of Technology, Rochester, NY, USA, 2007.
2. Zhu, E.; Zhao, J.; Li, B.; Gao, H. Trajectory planning for the powered parafoil at insufficient height. In Proceedings of the 33rd Chinese Control and Decision Conference, Kunming, China, 22–24 May 2021.
3. Li, B.; Qi, J.; Lin, T.; Mei, S.; Han, J. Real-Time Data Acquisition and Model Identification for Powered Parafoil UAV. In Proceedings of the 8th International Conference on Intelligent Robotics & Applications, Portsmouth, UK, 24–27 August 2015.
4. Ghoreyshi, M.; Bergeron, K.; Jirasek, A.; Seidel, J.; Lofthouse, R.J.; Cummings, R.M. Computational aerodynamic modelling for flight dynamics simulation of ram-air parachutes. *Aerosp. Sci. Technol.* **2016**, *54*, 286–301. [[CrossRef](#)]
5. Tao, J.; Dehmer, M.; Xie, G.; Zhou, Q. A generalized predictive control-based path following method for parafoil systems in wind environments. *IEEE Access* **2019**, *7*, 42586–42595. [[CrossRef](#)]
6. Zhu, E.; Gao, H.; Zhao, J. Trajectory planning of the powered parafoil based on multi-phase design. *J. Jiangsu Univ. Technol.* **2020**, *26*, 28–35.
7. Yang, H.; Song, L.; Liu, C.; Huang, J. Study on powered-parafoil longitudinal flight performance with a fast estimation model. *J. Aircr.* **2013**, *50*, 1660–1668.
8. Aoustin, Y.; Martinenko, Y. Control algorithms of the longitude motion of the powered paraglider. In Proceedings of the ASME 11th Biennial Conference on Engineering Systems Design and Analysis, Nantes, France, 2–4 July 2012.
9. Chen, S.; Sun, Q.; Luo, S. Longitudinal Control of Unmanned Powered Parafoil with Precise Control Gain. In Proceedings of the 13rd Chinese Intelligent Systems Conference, Mudanjiang, China, 14–15 October 2017.
10. Chen, Z.; Zhang, H. Altitude control for unmanned powered parafoil based on backstepping method. In Proceedings of the 28th Chinese Control and Decision Conference, Yinchuan, China, 28–30 May 2016.
11. Chen, Z.; Zhang, H.; Qiu, J.; Su, L. Adaptive backstepping altitude control for unmanned powered parafoil. *Control. Eng. China* **2018**, *25*, 554–558.
12. Tan, P.; Sun, Q.; Jiang, Y. Trajectory tracking of powered parafoil based on characteristic model based all-coefficient adaptive control. *J. Cent. South Univ.* **2017**, *24*, 1073–1081. [[CrossRef](#)]
13. Zhu, E.; Gao, H. Guidance-based path following control of the powered parafoil. *Control Eng. Appl. Inf.* **2020**, *22*, 42–50.
14. Hu, K-Y.; Wang, X.; Yang, C. Hybrid adaptive dynamic inverse compensation for hypersonic vehicles with inertia uncertainty and disturbance. *Appl. Sci.* **2022**, *12*, 11032. [[CrossRef](#)]
15. Wang, C.; Du, Y. Lane-Changing strategy based on a novel sliding mode control approach for connected automated vehicles. *Appl. Sci.* **2022**, *12*, 11000. [[CrossRef](#)]
16. Du, Y.; Cao, W.; Wu, M.; She, J.; Fang, M.; Kawata, S. Disturbance rejection and control system design using improved equivalent-input-disturbance approach. *IEEE Trans. Ind. Electron.* **2020**, *67*, 3013–3032. [[CrossRef](#)]
17. Du, Y.; Cao, W.; She, J.; Wu, M.; Fang, M.; Kawata, S. Disturbance Rejection and Robustness of Improved Equivalent-Input-Disturbance-Based System. *IEEE Trans. Cybern.* **2022**, *52*, 8537–8546. [[CrossRef](#)] [[PubMed](#)]
18. Guettal, L.; Chelihhi, A.; Ajgou, R.; Touba, M. Robust tracking control for quadrotor with unknown nonlinear dynamics using adaptive neural network based fractional-order backstepping control. *J. Franklin Inst.* **2022**, *359*, 7337–7364. [[CrossRef](#)]

19. Pouzesh, M.; Mobayen, S. Event-triggered fractional-order sliding mode control technique for stabilization of disturbed quadrotor unmanned aerial vehicles. *Aerosp. Sci. Technol.* **2022**, *121*, 107337. [[CrossRef](#)]
20. Zhu, E.; Sun, Q.; Chen, Z.; Kang, X.; He, Y. Modeling of powered parafoil based on kirchhoff motion equation. *Nonlinear Dyn.* **2015**, *79*, 617–629. [[CrossRef](#)]
21. Chen, Z.; Sun, M.; Yang, R. On the stability of linear active disturbance rejection control. *Acta Autom. Sin.* **2013**, *39*, 574–580. [[CrossRef](#)]
22. Shao, X.; Wang, L.; Li, J.; Liu, J. High-order ESO based output feedback dynamic surface control for quadrotors under position constraints and uncertainties. *Aerosp. Sci. Technol.* **2019**, *89*, 288–298. [[CrossRef](#)]
23. Das, S. *Functional Fractional Calculus*, 2nd ed.; Springer: Berlin, Germany, 2011; pp. 204–206.
24. Monje, C.; Chen, Y.; Vinagre, B.; Xue, D.; Feliu, V. *Fractional-Order Systems and Controls: Fundamentals and Applications*; Springer: London, UK, 2010; pp. 153–155.
25. Roy, P.; Roy, B. Sliding mode control versus fractional-order sliding mode control: Applied to a magnetic levitation system. *J. Control Autom. Electr. Syst.* **2020**, *31*, 597–606. [[CrossRef](#)]